THE JOURNAL OF PHYSICAL CHEMISTRY C

Article

Cite This: J. Phys. Chem. C 2018, 122, 17777−17783

pubs.acs.org/JPCC

Electrohydrodynamic Assembly of Ambient Ion-Derived Nanoparticles to Nanosheets at Liquid Surfaces

Depanjan Sarkar,[†] Rajesh Singh,[‡] Anirban Som,[†] C. K. Manju,[†] Mohd Azhardin Ganayee,[†] Ronojoy Adhikari,*[,‡,§] and Thalappil Pradeep*[,†]

[†]DST Unit of Nanoscience (DST UNS) and Thematic Unit of Excellence (TUE), Department of Chemistry, Indian Institute of Technology Madras, Chennai 60036, India

[‡]The Institute of Mathematical Sciences, HBNI, CIT Campus, Chennai 600113, India

[§]Department of Applied Mathematics and Theoretical Physics (DAMTP), Centre for Mathematical Sciences, University of Cambridge, Wilberforce Road, Cambridge CB3 0WA, United Kingdom

Supporting Information

ABSTRACT: We describe an ambient ion-based method to create free-standing metal nanosheets, which in turn are composed of nanoparticles of the corresponding metal. These nanoparticle-nanosheets (NP-NSs) were formed by the electrospray deposition (ESD) of metal ions on a liquid−air interface leading to nanoparticles that self-organize under the influence of electrohydrodynamic flows, driven by the electric field induced by the applied potential. Such a two-dimensional organization of noble metals is similar to the assembly of molecules at liquid−air interface and has the possibility of creating a category of new materials useful for diverse applications. Enhanced catalytic activity of the formed NP-NSs for Suzuki−Miyaura coupling reaction was demonstrated, which was attributed to their large surface-to-volume ratios.

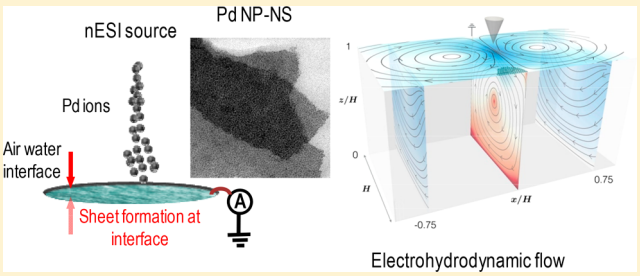

1. INTRODUCTION

Molecular interactions at liquid−air interfaces have been investigated from the times of Agnes Pockels.[1−3] Structures assembled at liquid−air interfaces and subsequently transferred to solid surfaces have contributed to the understanding of two-dimensional (2D) films of diverse materials.[4−16] While stable molecules and particles arrange at the interface due to surfactancy, it is possible to create nanostructures at the interface directly, starting from atomic precursors. A new methodology introduced recently to synthesize metal NPs on solid surfaces by ambient electrolytic spray[17,18] as well as electrospray[19] can be adapted to liquid surfaces leading to synthesis and assembly simultaneously without the use of reducing agents. Electrospray has been used earlier to assemble polymer beads at liquid surfaces.[20] Superiority of electrolytic spray (direct ionization of noble metals from the corresponsing electrodes by electrochemical corrosion) and electrospray (ionization of metal ions from its precursor salts) to make metal NPs over previous methods[21−24] lies in the fact that they do not involve any components other than the metal precursors. This ambient and direct method of synthesis is less expensive in comparison to processes like physical vapor deposition (PVD) (used for synthesis of metal NPs)[22,25] as no sophisticated instrumentation is used. Most important advantage of this method is that it can be performed at room temperature in air. On the other hand, a technique like PVD, a well-studied technique for creating diverse variety of thin films, can be performed in vacuum at elevated temperatures but has more precision (in terms of thickness control) over this ambient technique. Ambient electrospray deposition (ESD), being a very new technique for materials synthesis, offers new possibilities in terms of easy manipulation of concentrations, variation of mixtures to create alloys, incorporation of soluble precursors, etc. Parameters like deposition rate, deposition time, distance from the nESI tip to the collector surface, etc. have similarities with PVD operations. Atmospheric processing offers various advantages in the utilization of the film as in the case of catalysis. Along with several advantages, the method comes with a disadvantage of lack of precise control over the thickness of the 2D sheets. Controlling ionization efficiency, nature of ions formed, purity of the ions, etc., can cause limitations in the film deposited. The presence of an electrical double layer at the liquid−air interface and its mobility in response to moderate electric fields can drive directed motion at both the surface and the bulk of the liquid which, in turn, can guide suspended NPs into ordered assemblies.

With this objective, we performed a series of experiments by which NPs of Pd were synthesized, without any reducing agent, on the surface of a water reservoir which then self-

Received: May 2, 2018
Revised: July 16, 2018
Published: July 16, 2018

DOI: 10.1021/acs.jpcc.8b04169
J. Phys. Chem. C 2018, 122, 17777−17783

assembled to form nanoparticle-nanosheets (NP-NSs). Visualization of the surface and bulk motion of the liquid, using colored dyes, suggested that fluid flow is the principal mechanism underlying this spontaneous assembly, which has been modeled below. The resulting free-standing NP-NS was used for applications such as heterogeneous catalysis for C−C bond formation. Pd is well-known as a catalyst for C−C bond formation. Here we show enhanced activity of the 2D NP-NSs due to their high active surface area. The simplicity and versatility of this methodology, which allows for diverse precursors and varying liquids, opens up the possibility of creating a rich variety of nanoscale materials for studying novel physicochemical phenomena.

2. EXPERIMENTAL DETAILS

In all our deposition experiments, electrospray deposition was used. Electrospray deposition experiments were performed using a homemade nanoelectrospray (nESI) setup. A borosilicate glass capillary of 1.5 mm outer diameter and 0.86 mm inner diameter was pulled into two parts leaving an opening of 15−20 μm, at the tip. These microtips, filled with the precursor solution, were used as the ion source. A positive DC potential of 1.5−2.5 kV was applied through a platinum (Pt) wire electrode to generate the electrospray. The Pt wire was immersed into the precursor solution. The electrospray plume, ejected from the tip of the glass capillary, was collected over a grounded liquid surface (deionized water (DI) water taken in a 1 mL plastic vial) to synthesize NP-NSs. A copper strip stuck on the inside wall of the vial was connected to the ground through a picoammeter; hence the copper strip works as the ground electrode. 5 mM solutions of $PdCl_2$, $Au(OAc)_3$ in acetonitrile and AgOAc in water were used as precursors for the respective metals. In the cases of Pd and Au, DI water was used as the deposition surface, and in the case of Ag, it was changed to ethylene glycol (EG). We have deposited Pd and Au on water as the precursor salts are insoluble in water. In the cases of Ag and Ni, the liquid was changed from water to ethylene glycol (EG) to ensure reduced solubility of AgOAc and Ni(II) acetate tetrahydrate, used as the precursors for Ag and Ni, respectively. In contrast, when water was used as a deposition substrate, Ag NPs did not form the nanosheet. The liquid surface was grounded through a picoammeter to measure the deposition current. All deposition experiments were performed at a typical deposition current of 60−70 nA. After a certain time of deposition, a thin layer was seen floating on the liquid surface, which was found to be a metal sheet made of NPs. As we used nESI for deposition for all our experiments, spreading of solvent may not have much role in the observed process. In the case of nESI, the size of droplets is very small. Hence, when they travel a distance of around 10 mm from the source to deposit on the liquid surface, most of the solvent evaporates.

3. RESULTS AND DISCUSSION

Experiments were conducted as shown in Figure 1A, wherein a nanoelectrospray ion (nESI) source gently deposits ions (at 60−70 nA) on a grounded liquid surface. Experimental details of the methodology are described in the section Experimental Details and Supporting Information. A schematic representation of the experimental setup with complete dimensional details is shown in Figure S1, Supporting Information. At first, we collected the mass spectrum (Figure 1B) from an

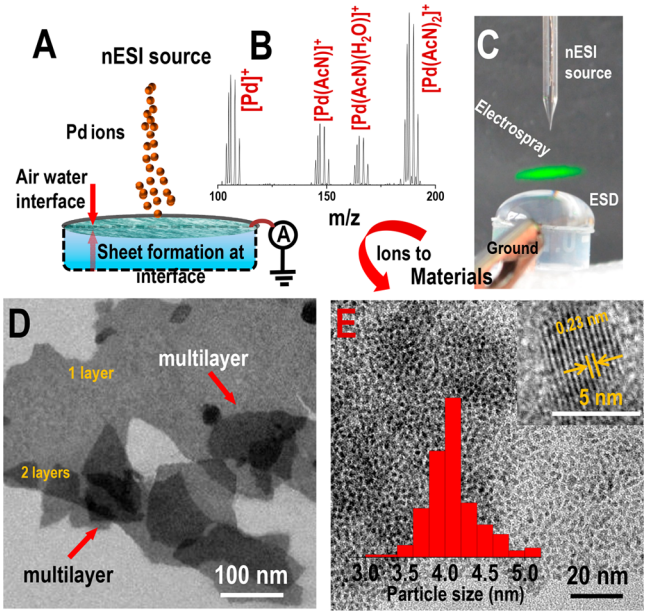

Figure 1. (A) Schematic of the electrospray deposition of $PdCl_2$ on water surface, (B) mass spectrum of $PdCl_2$ solution in acetonitrile, collected using nESI source, and (C) optical photograph of electrospray deposition at air−water interface. The electrospray was visualized using a green laser pointer showing scattering from the droplets. Liquid was grounded by a metal clip. (D, E) TEM images of the formed Pd NP-NS collected from the liquid surface after washing with water, at different magnifications. Inset of (E) shows HRTEM image of Pd sheet showing that it is made of nearly uniform crystalline Pd NPs and a size distribution histogram for the Pd NPs.

electrosprayed solution of $PdCl_2$ in acetonitrile (AcN). Peaks corresponding to Pd^+ and solvated Pd^+ ions such as $[Pd(AcN)]^+$, $[Pd(AcN)(H_2O)]^+$, and $[Pd(AcN)_2]^+$ with their characteristic isotopic patterns confirm that the droplets generated in electrospray contain Pd in its +1 state. Electrospray, being reducing in nature, converts Pd(II) to Pd(I) within the charged droplets (Figure 1B). These Pd^+ ions along with the counteranions (Cl^- in this case) were deposited on a grounded water surface. The spray plume also contains salt clusters (Figure S2), but the major species are metal ions and their solvated ions. The counteranions go into the water and the metal ions get reduced to form the NPs (discussed in detail below). A copper strip was attached to the wall of the container and it was grounded through a picoammeter. In the course of deposition, Pd^+ ions got reduced to Pd(0) by taking electrons from the grounded electrode. Figure 1C shows an optical photograph of the deposition process. A green laser pointer was shone on the spray plume for its better visualization. After 1 h of deposition at a deposition current 40 nA, an orange colored film was seen floating on water. This film was collected on different substrates by scooping it from water and was characterized using various techniques. Figure 1D shows a TEM image of clean Pd NP-NSs. Detailed TEM imaging was performed to prove that the sheet was made of Pd NPs. Figure 1E shows a TEM image of the as-synthesized Pd NP-NSs, and inset shows a high-resolution transmission electron microscopic (HRTEM) image of the NPs present in the sheet, respectively. Figure 1E clearly shows the presence of monodisperse Pd NPs in the sheet. The average size of Pd NPs was around 4 nm. Inset of Figure 1E shows a size distribution histogram for the NPs. The lattice distance of these NPs

DOI: 10.1021/acs.jpcc.8b04169
J. Phys. Chem. C 2018, 122, 17777−17783

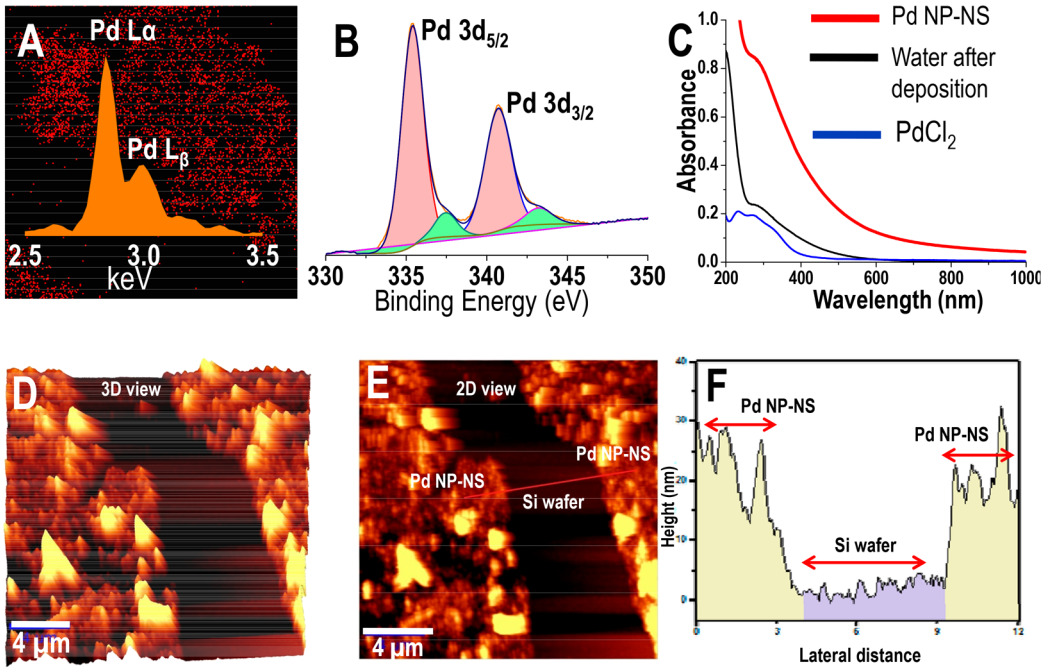

Figure 2. (A) EDS mapping and spectrum of the Pad NP-NSs, showing the presence of only Pd, (B) X-ray photoelectron spectrum showing that Pd is in its zero valence state with slight contribution from a surface oxide layer, (C) UV−vis spectra of Pd NP-NS, water after Pd deposition and $PdCl_2$ in ACN. For the Pd sheet, as there is scattering, the *Y* axis may be taken as extinction. (D, E) AFM images of the Pd NP-NSs and (F) height profile taken across the red line in (E). 3D views are shown to illustrate the roughness. The image was taken deliberately by including a crack in the film to measure the film thickness. The film was taken on a silicon wafer.

matches with the (111) plane of Pd, proving the metallic nature of the Pd NPs. The deposited Pd ions were neutralized at the interface and aggregated to form Pd NPs.

Monodispersity of the NPs suggests that the uniformity of the droplets has a significant role in controlling the particle size because the uniform droplets may contain identical number of metal ions, which in turn make the NPs after reduction. The NPs were assumed to be born as soon as the charged droplets, containing similar number of ions, impacted the water surface. We can calculate the number of atoms present in a 4 nm Pd NP and correlate that to the droplet size. From the literature of size distribution of electrosprayed droplets, we know that in the case of acetonitrile, the charged droplets are approximately 700 nm in diameter. These droplets shrink (within 3.5 ms) to 100 nm size while traveling in air.[26] In our case, we assume the droplets that reach the surface of the water after 10 mm travel in air are 250 nm in size. Hence the volume of the droplet is 8.1×10^{-15} mL. The number of Pd ions present in the droplet considering the concentration of the Pd solution (5 mM) is 24 486. The number of atoms present in a 4 nm Pd NP is around 26 000 (considering 137 pm as the metallic radius of Pd). These two numbers are close enough to conclude that the droplet size is a very important factor for the monodispersity of the NPs, although further efforts are needed to verify this aspect, and we are continuing to investigate this. We performed other measurements to understand the material better.

Energy dispersive spectroscopic (EDS) analysis of the same shows the presence of only Pd in the sheet (Figure 2A). A detailed EDS spectrum is presented in Figure S3, where no impurities are detected. Hence we speculate that the chloride ions (counterpart of the precursor) go into the water reservoir. This was proved by measuring the conductivity of the water with respect to deposition time (Figure S4); the plot shows a linear enhancement. Figure 2B shows the X-ray photoelectron spectrum (XPS) of Pd NP-NSs with peaks due to Pd $3d_{5/2}$ (335.4 eV) and Pd $3d_{3/2}$ (340.7 eV), which support the presence of Pd(0). The XPS spectrum does not show the presence of any other species like chlorine, proving that these particles are unprotected. For the XPS study, more material was collected on the sample plate by collecting the NP-NS multiple times. EDS spectrum collected from the Pd NP-NSs (Figure S3) shows that the NSs are made of 100% Pd. There are no organic substances present as protecting species. Hence, we believe that the NPs are bare metal particles. We see the presence of small amounts of oxygen in EDS and a weak feature due to Pd^{2+} in XPS. This surface oxide may be the bridge for the NPs to form NSs, along with van der Waals forces. Figure 2C shows the UV−vis spectra of the Pd NP-NSs (red trace, solid state UV−vis spectrum of Pd NP-NS, coated on a quartz coverslip), the water on which the deposition happened (black trace), and the precursor $PdCl_2$ solution (blue trace).

The difference between the blue and red traces clearly proves that the salt solution has transformed to metal NPs upon ESD, at room temperature. The hump near 300 nm is a characteristic feature of Pd NPs due to the plasmonic excitation, which occurs around 340 nm for naked Pd NPs in a pure dispersion in toluene (0.2 mg/mL).[27] The UV−vis spectrum of the water after deposition (black trace) also shows the same feature corresponding to Pd NPs. This implies that some portion of Pd NPs goes into the water due to the generated flow field in water, whereas most of them stay at the interface and arrange to form Pd NP-NSs. Quantitative analysis shows that approximately 85% of the Pd comes at the surface. This metallic sheet can be made over a large area; Figure S5A shows a TEM image of such a NP-NS over an area of 80 μm^2. The image shows the presence of excess Pd on the sheet, due

DOI: 10.1021/acs.jpcc.8b04169
J. Phys. Chem. C 2018, 122, 17777−17783

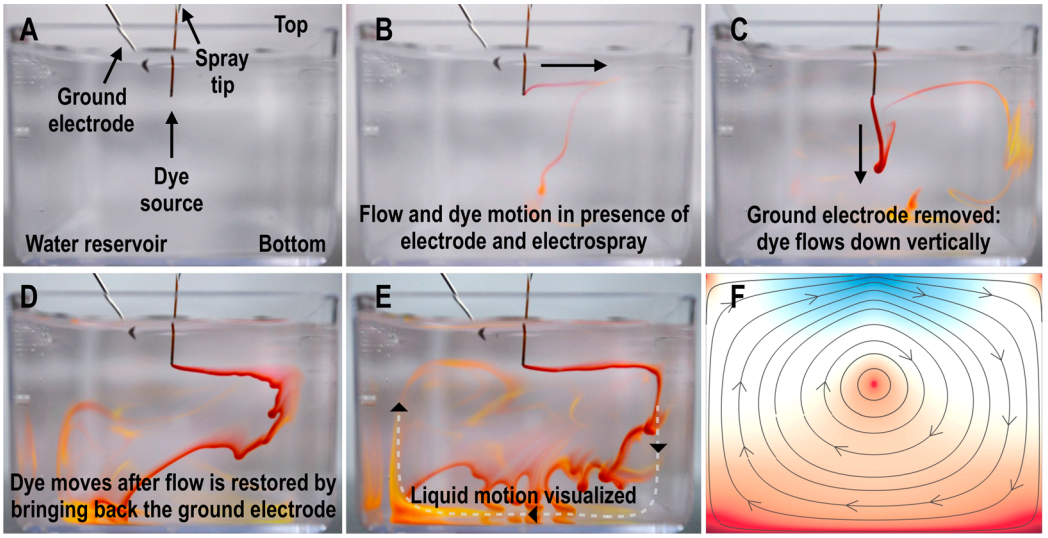

Figure 3. (A) Electrospray deposition setup. (B) Advection of the dye by the flow when the spray is present. (C) Cessation of flow, with the dye falling vertically, when the spray is absent. (D) Resumption of the advection as the spray is again turned on and (E) circulation of the dye as it is carried along by the fluid streamlines. (F) Streamlines of a theoretically computed flow which compares well with circulation seen in (E).

to longer deposition time, which can be removed by washing with deionized (DI) water. The sheets can be scooped out of the liquid surface with a spatula or coverslip or similar supports. After the ESD synthesis, the as-synthesized Pd NP-NSs were collected and washed with DI water by taking them in an Eppendorf vial and shaking the vial manually. Figure S5B shows the TEM image of the same sheet after washing. In this case, we see very clean sheets of Pd made of Pd NPs. The sheet was broken into small parts after washing, retaining their morphology, proving the stability of these NP-NSs. When the film thickness is large, the film could resist mechanical damage. Control experiments were performed for better understanding the phenomena as will be discussed below. Here, we speculate that the electron transfer from the grounded electrode to the metal ions was assisted by the hydroxyl ions (OH^-). High mobility of the OH^- ions resulted in fast transfer of electrons, leading to the formation of uniform Pd NPs at the water surface. OH^- ions are also responsible for the formation of a mobile electrical double layer which drives an electro-hydrodynamic flow at both the surface and the bulk of water.

The Pd NPs move in the flow field (see below) and arrange themselves to form a thin nanosheet at the air−water interface. A quantitative theory of this phenomenon is provided below. Atomic force microscopy (AFM) was performed on the Pd NP-NSs to understand the thickness. Figure 2D and Figure 2E show the AFM images of the Pd NP-NSs, in 3D and 2D views, respectively. Figure 2F shows a height profile of a Pd NP-NS showing an average thickness of 26 nm and a roughness of ±12 nm. The thickness presented above is calculated from the AFM image. In a typical thickness of 26 nm, the NP-NSs contain approximately four monolayers. However, the thickness of the layers formed on the liquid surface may be different as the film may get modified during the process of sample preparation.

Although the assembly of the NPs is not highly ordered so that it can be named as hexagonal assembly, deposition at a very low deposition current, i.e., a slow deposition rate, leads to a relatively better-ordered structure, whereas a fast deposition leads to an increased disorder. Figure S6A and Figure S6B show TEM images of Pd NP-NSs synthesized by slow (30 nA) and fast (80 nA) ESD conditions, respectively. Such a current can be carried by the residual OH^- ions present (6.023×10^{16} ions/L) in neutral water. A control experiment was performed to show the role of OH^-. ESD of acetonitrile solution of $PdCl_2$ was performed under the same conditions. In this case the deposition was over acidic pH (pH 4) and no NP-NSs were observed (Figure S7). At low pH due to the lack of OH^- ions, the precursor salt did not reduce completely to form Pd NPs. Hence the metal ions did not neutralized completely and as a result they combined with their counterions and remained as salt after deposition, on top of the liquid which can be seen in the TEM image and EDS spectrum in Figure S7A, although part of it was reduced to form crystalline NPs as shown in Figure S7B. Due to the salt deposition, free movement of the bare NPs was hindered leading to aggregation instead of 2D assembly of NSs. Free-standing metal NP-NSs were made using other metals also. Parts A, B, and C of Figure S8 show the TEM images of NP-NSs made of silver, gold, and nickel, respectively. In the case of gold, an acetonitrile solution of Au(III) acetate was electrosprayed on water. Just like the case of Pd, formation of a thin film was seen at the air−water interface. The thin film was collected on a TEM grid for characterization. The more common $HAuCl_4$ salt was not suitable as it exists as H^+ and $AuCl_4^-$ in solution and does not form NPs by this process. From experiments discussed in the Supporting Information, we know that the solubility of the precursor salt, dispersibility of the formed NPs, and surface tension of the liquid substrate play crucial roles in the NP-NS formation. Ag NP-NSs were synthesized using other silver precursors like silver nitrate and silver perchlorate (Figure S9).

ESD was also performed with a mixture of precursors to make bimetallic NP-NSs. In this experiment, mixed precursor solutions of two different metals (Ag−Pd and Au−Pd) were electrospray deposited on top of the water surface. 10 mM solutions of silver acetate (in water), palladium chloride (in ACN), and 5 mM solution of gold acetate (in ACN) were used as precursors. All other experimental parameters were identical to the previous experiments. Figure S10A and Figure S10B show the TEM images taken after ESD of Au−Pd and Ag−Pd mixtures, respectively. It is evident from the TEM images that the metal NPs were assembled and phase separated. The

DOI: 10.1021/acs.jpcc.8b04169
J. Phys. Chem. C 2018, 122, 17777−17783

mobilities of different ions may play crucial roles in separating them. EDS mapping (Figure S10C–F) images clearly show that the NPs aggregated separately, when deposited from a mixed precursor solution. It appears that the kinetics of reduction of different metals by this method is different which results in phase separation than alloying.

The above experimental results demonstrate that NP-NS formation is robust against alterations of metal in the electrospray and the liquid on whose surface the spray falls. Thus, generic physical mechanisms rather than specific chemical mechanisms must be at play, which leads us to the following conjecture. Spray deposition creates additional ionic species in the liquid, a fraction of which are adsorbed at the liquid–air interface, producing a strongly charged electrical double layer.[28] It is known, for instance, that such a double layer forms at room temperature at the air–water interface with a negative ζ-potential of a few tens of millivolts. The tangential electric field at the liquid–air interface provides an electromotive force on the double layer, setting it in motion along the electric field if the ζ-potential is positive and opposite to it if the ζ-potential is negative. Viscous stresses in the liquid set adjacent fluid layers into motion which then develops into a steady-state fluid flow with a circulatory character, the latter property being a consequence of finite compressibility and container volume. The flow can continuously advect NPs dispersed in the bulk of the liquid to the liquid–air interface, and its surface component can guide NPs to assemble into packed structures.

To test the validity of this conjecture, we visualize the surface and bulk flow in the liquid both in the presence and in the absence of electrospray, as shown in Figure 3. The flow experiment was shown in a square shaped container for the following two reasons: (i) calculations were performed assuming a square shape container as the collector for ESD and (ii) to prove that the shape of the container does not have any effect in the formation of the NSs. We maintained an identical distance between the center of the spray and the ground electrode in both the cases. The experimental setup is shown in panel A. In the presence of electrospray, the dye does not fall vertically, as would be expected, but is advected tangential to the liquid–air interface; see panel B. In contrast, when the spray is absent by removing the ground electrode, the dye falls vertically under gravity, with no detectable tangential convection; see panel C. The tangential convection resumes when the spray is restored and the process can be repeated at will with completely predictable results; see panels E and F. The general circulatory pattern of the bulk fluid flow reveals itself once the dye is transported along the fluid streamlines, given a sufficient duration of spraying (see video S1 provided in Supporting Information). We have also shown the flow of the liquid at the surface using both experimental and theoretical surface flow. As shown in the Figure S11 (and in video S2), the combined effect of electrospray and tangential electric field from the electrode leads to a convective flow field in which the particles are driven to the edge of the container (opposite the electrode). The electrohydrodynamic flow brings the particles within the range of the short-range attraction and packs the particles into a 2D sheet.[29] Once the particles are packed to form the 2D sheet, the film formed is stabilized by a tiny oxide layer present between the particles. This is the reason for the particles not to fall apart once the flow is off.

Figure 4 shows the results of a theoretical computation of these streamlines, which is in excellent qualitative agreement

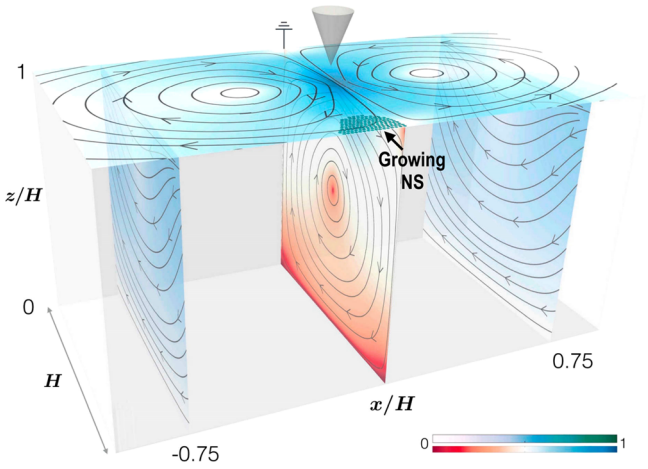

Figure 4. Theoretically computed streamlines of electrohydrodynamic flow in long channel whose cross section is a square of sides H. The spray from the cone above deposits charges at the air–liquid interface which are then set into motion by the tangential electric field. For a negative interfacial ζ-potential, the resulting flow puts NS away from the ground electrode. The bulk fluid, though electrically neutral, is set into motion due to viscous stresses. The combined action of the surface and bulk flow guides the nanoparticles into ordered aggregates at the edge of the channel opposite the electrode.

with the experiment. We now outline the quantitative aspects of the electrohydrodynamic computation that yields the streamlines. The basis of our computations is the electrohydrodynamic system of equations first proposed by Taylor and Melcher,[30] where conservation of fluid momentum and electric charge are combined with constitutive equations for the mechanical and electrical stress, assuming that the fluid is mechanically Newtonian (viscosity η) and electrically a linear dielectric (permittivity ϵ) and an ohmic conductor (conductivity σ).

In the regime of slow viscous flow relevant to the present experiment, this implies

$$\nabla\cdot(\mathbf{T}^{m} + \mathbf{T}^{e}) = 0 \tag{1}$$

where $T_{ij}^{m} = -p\delta_{ij} + \eta_{ijkl}\nabla_k v_l$ and $T_{ij}^{e} = \epsilon \mathrm{E}_i E_j - {}^1/_2\epsilon E^2\delta_{ij}$ are, respectively, Cartesian components of the mechanical and electrical stress tensors, v_i and E_i are the Cartesian components of the fluid flow. The fluid flow is assumed to be incompressible, $\nabla\cdot\mathbf{v} = 0$, and the electric field is assumed to be irrotational, $\nabla \times \mathbf{E} = 0$. With the constitutive equations, $\mathbf{D} = \epsilon\mathbf{E}$, for the displacement $\mathbf{D}$ and $\mathbf{J} = \sigma\mathbf{E}$ for the current density $\mathbf{J}$, the electric charge distribution ρ obeys the Maxwell and continuity equations

$$\nabla\cdot\mathbf{D} = \rho \tag{2}$$

$$\partial_t\rho + \nabla\cdot(\mathbf{J} + \rho\mathbf{v}) = 0 \tag{3}$$

and the above three coupled systems of equations, when supplemented by interfacial boundary conditions, determine the fluid flow, electric field, and charge distribution.

We solve the above equations in a rectangular channel of square cross section whose length is much greater its width H. We assume the limit in which the charge relaxation time $\tau = \epsilon/\sigma$ ($\sim 10^{-5}$ s for water) and the flow time scale $\tau' = \eta H/\gamma$ ($\sim 10^{-4}$ s for water, where γ is the surface tension) are both rapid compared to the remaining time scales so that the bulk is electroneutral and all free charges are confined to the interface.

DOI: 10.1021/acs.jpcc.8b04169
J. Phys. Chem. C 2018, 122, 17777–17783

We assume a constant tangential electric field and a Gaussian free charge density profile $\rho(\mathbf{r}) \sim \exp[-r^2/(2a^2)]$ where a is the characteristic width. We ensure that the ratio a/H matches experiment. Then, the fluid flow can be expressed as an integral over all boundaries as

$$\mathbf{v}(\mathbf{r}) = \int \mathbf{G}(\mathbf{r}, \mathbf{r}')\cdot\mathbf{f}^S(\mathbf{r}')\, dS + \int \mathbf{K}(\mathbf{r}, \mathbf{r}')\cdot\mathbf{n}\mathbf{v}^S(\mathbf{r}')\, dS \quad (4)$$

where $\mathbf{f}^S = \rho\mathbf{E}$ is the interfacial force density, $\mathbf{v}^S$ is the interfacial velocity, $\mathbf{G}$ is a Green's function of Stokes flow, and $\mathbf{K}$ is its associated stress tensor. The integral can be completed following procedures outlined in the Supporting Information, and the streamlines of the flow can be numerically computed. The result of the above computation is shown in Figure 4. The circulatory streamlines are clearly visible in both the bulk and surface flows which are, as explained above, central to the mechanism of self-assembly of NPs.

Pd in its zero oxidation state is very well-known for catalyzing C−C bond formation reactions. Hence, the catalytic activity of the synthesized Pd NP-NS was tested for the Suzuki−Miyaura coupling reaction. For this, the as-synthesized Pd NP-NSs were taken on quartz coverslips and dipped into a reaction mixture of a boronic acid and an organohalide. An aqueous solution of Na_2CO_3 was added to the reaction mixture to make it basic in nature. After the addition of the catalyst, the reaction mixture was stirred in a round-bottom flask at room temperature and the product was analyzed using mass spectrometry.

Figure 5 shows a mass spectrum of the reaction mixture containing 4-bromophenol (reactant I) and 4-tolylboronic acid

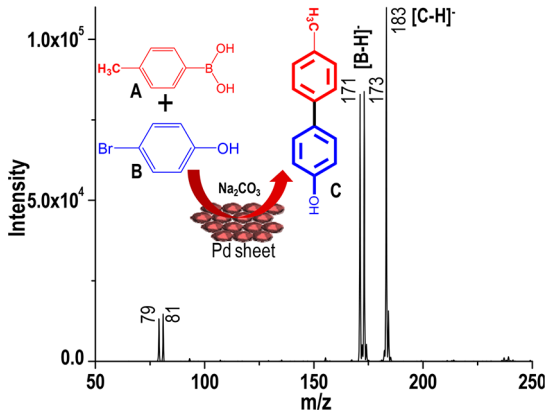

Figure 5. Mass spectrum collected after Pd NP-NS catalyzed coupling reaction between 4-tolylboronic acid and 4-bromophenol. Inset shows the structures of the reactants and the product.

(reactant II) in the presence of Pd NP-NS (0.02 mg) catalyst after 30 min of stirring. Intense peak at m/z 183 in the mass spectrum corresponds to the reaction product, i.e., 4′-methyl[1,1′-biphenyl]-4-ol (III). The inset shows the molecular structures of the reactants and the product. The mass spectrum also shows two peaks for II at m/z 171 and 173, due to the equal abundance of the isotopes of Br. Sodium bromide (NaBr) is a byproduct in this reaction leading to the presence of peaks corresponding to bromide ion (Br^-) in the mass spectrum (peaks at m/z 79 Br^- and 81 Br^-).

Control experiments were performed to prove that the Pd NP-NS catalyst is essential for the coupling reaction. The mass spectrum (Figure S12A) collected from a mixture of the same reactants, without a catalyst, after 30 min did not show any peak other than the reactants. A comparative study was also carried out to estimate the efficiency of our catalyst. In this experiment, commercially available tetrakis(triphenylphosphine)palladium(0) was used as the catalyst (1 mg) for one set of reaction (reaction mixture X). In the other set (reaction mixture Y), Pd NP-NS was used as the catalyst. All the other parameters such as the concentration of the reactants, solvent, temperature and reaction time were kept constant in both the cases. Figure S12B and S12C show the mass spectrum collected from the reaction mixtures X and Y, respectively, after 30 min of stirring. The efficiency (calculated considering only the metal percentage in both the cases) of Pd NP-NS catalyst was approximately 23 times higher than the commercial catalyst. The 2D nature and surface roughness exposing more catalytically active sites may be attributed as the main reason for higher efficiency. From the AFM data (Figure 2D and Figure 2E) it is also evident that the surface of the NP-NSs is highly rough. It was tested for C−C coupling reactions for various boronic acids and organic halides (see Table S1, Figure S13, and S14). UV−vis spectroscopy also supports the C−C bond formation showing a broad hump around 450 nm (the red trace in Figure S15), a characteristic feature of biphenyl compounds. All the data presented here prove that the Pd NP-NSs are more efficient catalysts for Suzuki−Miyaura coupling reaction. Stability and reusability of the catalyst were also checked using UV−vis spectroscopy and TEM imaging. A detailed description of this is given in the Supporting Information (Figure S16).

4. CONCLUSIONS

In summary, we report an ambient ion based method of making free-standing 2D metal sheets made of bare NPs, at the liquid−air interface. An electrohydrodynamic flow field was generated by ESD on the liquid surface, which in turn assisted the assembly of the NPs. This is the first report of generating such a flow field in fluids using ESD. The NP-NSs were made under ambient conditions at room temperature from metal salt precursors. We showed that such sheets can be made of different elements such as Pd, Au, Ag, and Ni. Synthesized 2D NP-NSs were used as efficient and reusable heterogeneous catalysts for C−C bond formation reactions. The methodology suggested can be used for organized nanoscale films of metals under ambient conditions. The structure and composition of the assemblies can be varied easily to obtain new properties.

■ ASSOCIATED CONTENT

Supporting Information

The Supporting Information is available free of charge on the ACS Publications website at DOI: 10.1021/acs.jpcc.8b04169.

Experimental details, schematic representation of the experimental setup; detailed TEM EDS spectrum of Pd NP-NSs; plot of conductivity of bulk water, on whose surface deposition happened, vs deposition time; TEM image of Pd NP-NS before and after washing with DI water; TEM images of Pd NP-NS synthesized by slow and fast electrospray deposition; TEM images of Pd NPs formed after ESD of $PdCl_2$ on formic acid solution; TEM images of NP-NSs made of silver, gold, and nickel; TEM image of silver NP-NS made from silver perchlorate and silver nitrate; mass spectrum of control experiments, experimental and theoretical surface flows;

DOI: 10.1021/acs.jpcc.8b04169
J. Phys. Chem. C 2018, 122, 17777−17783

mass spectrum collected from the reaction mixtures (serial no. 2−5) mentioned in Table S1; mass spectrum collected from the reaction mixtures (serial no. 6−10) mentioned in Table S1; UV−vis spectrum; proof of stability and reusability of the catalyst; structures of reactants and products; theoretical details of electrohydrodynamic flow (PDF)
Video S1 of fluid flow visualization (AVI)
Video S2 of surface flow visualization (AVI)

AUTHOR INFORMATION

Corresponding Authors

*R.A.: e-mail, rjoy@imsc.res.in.
*T.P.: e-mail, pradeep@iitm.ac.in.

ORCID

Anirban Som: 0000-0002-6646-679X
Thalappil Pradeep: 0000-0003-3174-534X

Notes

The authors declare no competing financial interest.

ACKNOWLEDGMENTS

We thank the Nano Mission, Department of Science and Technology, Government of India, for continued support of our research program. D.S. and M.A.G. thank the University Grants Commission, A.S. and C.K.M. thank the Council of Scientific and Industrial Research for research fellowships.

REFERENCES

(1) Pockels, A. The angle of contact and the spreading of liquids on solid substances. *Phys. Z.* **1914**, *15*, 39−46.
(2) Reich, K. Out of the Shadows. Contributions of Twentieth-Century Women to Physics edited by Nina Byers and Gary Williams. *Acta Crystallogr., Sect. A: Found. Crystallogr.* **2008**, *64* (3), 432.
(3) Rayleigh. Surface Tension. *Nature* **1891**, *43*, 437.
(4) Natansohn, A.; Rochon, P. Photoinduced Motions in Azo-Containing Polymers. *Chem. Rev. (Washington, DC, U. S.)* **2002**, *102* (11), 4139−4175.
(5) Li, X.; Zhang, G.; Bai, X.; Sun, X.; Wang, X.; Wang, E.; Dai, H. Highly conducting graphene sheets and Langmuir-Blodgett films. *Nat. Nanotechnol.* **2008**, *3* (9), 538−542.
(6) Cote, L. J.; Kim, F.; Huang, J. Langmuir-Blodgett assembly of graphite oxide single layers. *J. Am. Chem. Soc.* **2009**, *131* (3), 1043−1049.
(7) Kim, J.; Cote, L. J.; Kim, F.; Yuan, W.; Shull, K. R.; Huang, J. Graphene Oxide Sheets at Interfaces. *J. Am. Chem. Soc.* **2010**, *132* (23), 8180−8186.
(8) Whang, D.; Jin, S.; Wu, Y.; Lieber, C. M. Large-Scale Hierarchical Organization of Nanowire Arrays for Integrated Nanosystems. *Nano Lett.* **2003**, *3* (9), 1255−1259.
(9) Fendler, J. H. Self-Assembled Nanostructured Materials. *Chem. Mater.* **1996**, *8* (8), 1616−1624.
(10) Kim, F.; Kwan, S.; Akana, J.; Yang, P. Langmuir-Blodgett nanorod assembly. *J. Am. Chem. Soc.* **2001**, *123* (18), 4360−4361.
(11) Lu, Y.; Liu, G. L.; Lee, L. P. High-Density Silver Nanoparticle Film with Temperature-Controllable Interparticle Spacing for a Tunable Surface Enhanced Raman Scattering Substrate. *Nano Lett.* **2005**, *5* (1), 5−9.
(12) Zasadzinski, J. A.; Viswanathan, R.; Madsen, L.; Garnaes, J.; Schwartz, D. K. Langmuir-Blodgett films. *Science (Washington, DC, U. S.)* **1994**, *263* (5154), 1726−33.
(13) Hammond, P. T. Form and function in multilayer assembly: New applications at the nanoscale. *Adv. Mater. (Weinheim, Ger.)* **2004**, *16* (15), 1271−1293.
(14) Langmuir, I.; Blodgett, K. B. A new method of investigating unimolecular films. *Kolloid-Z.* **1935**, *73*, 258−263.
(15) Blodgett, K. B. Monomolecular films of fatty acids on glass. *J. Am. Chem. Soc.* **1934**, *56*, 495.
(16) Lee, S.-L.; Lin, C.-H.; Cheng, K.-Y.; Chen, Y.-C.; Chen, C.-h. Stability of Guest-Incorporated 2D Molecular Networks. *J. Phys. Chem. C* **2016**, *120* (44), 25505−25510.
(17) Li, A.; Luo, Q.; Park, S.-J.; Cooks, R. G. Synthesis and Catalytic Reactions of Nanoparticles formed by Electrospray Ionization of Coinage Metals. *Angew. Chem., Int. Ed.* **2014**, *53* (12), 3147−3150.
(18) Li, A.; Baird, Z.; Bag, S.; Sarkar, D.; Prabhath, A.; Pradeep, T.; Cooks, R. G. Using Ambient Ion Beams to Write Nanostructured Patterns for Surface Enhanced Raman Spectroscopy. *Angew. Chem., Int. Ed.* **2014**, *53* (46), 12528−12531.
(19) Sarkar, D.; Mahitha, M. K.; Som, A.; Li, A.; Wleklinski, M.; Cooks, R. G.; Pradeep, T. Metallic Nanobrushes Made using Ambient Droplet Sprays. *Adv. Mater. (Weinheim, Ger.)* **2016**, *28* (11), 2223−2228.
(20) Nie, H.-L.; Dou, X.; Tang, Z.; Jang, H. D.; Huang, J. High-Yield Spreading of Water-Miscible Solvents on Water for Langmuir-Blodgett Assembly. *J. Am. Chem. Soc.* **2015**, *137* (33), 10683−10688.
(21) Quintanilla, A.; Valvo, M.; Lafont, U.; Kelder, E. M.; Kreutzer, M. T.; Kapteijn, F. Synthesis of Anisotropic Gold Nanoparticles by Electrospraying into a Reductive-Surfactant Solution. *Chem. Mater.* **2010**, *22* (5), 1656−1663.
(22) Sugioka, D.; Kameyama, T.; Kuwabata, S.; Torimoto, T. Single-step preparation of two-dimensionally organized gold particles via ionic liquid/metal sputter deposition. *Phys. Chem. Chem. Phys.* **2015**, *17* (19), 13150−13159.
(23) Sugioka, D.; Kameyama, T.; Kuwabata, S.; Yamamoto, T.; Torimoto, T. Formation of a Pt-Decorated Au Nanoparticle Monolayer Floating on an Ionic Liquid by the Ionic Liquid/Metal Sputtering Method and Tunable Electrocatalytic Activities of the Resulting Monolayer. *ACS Appl. Mater. Interfaces* **2016**, *8* (17), 10874−10883.
(24) Hamada, T.; Sugioka, D.; Kameyama, T.; Kuwabata, S.; Torimoto, T. Electrocatalytic activity of bimetallic Pd-Au particle films prepared by sequential sputter deposition of Pd and Au onto hydroxyl-functionalized ionic liquid. *Chem. Lett.* **2017**, *46* (7), 956−959.
(25) Anantha, P.; Cheng, T.; Tay, Y. Y.; Wong, C. C.; Ramanujan, R. V. Facile production of monodisperse nanoparticles on a liquid surface. *Nanoscale* **2015**, *7* (40), 16812−16822.
(26) Wortmann, A.; Kistler-Momotova, A.; Zenobi, R.; Heine, M. C.; Wilhelm, O.; Pratsinis, S. E. Shrinking Droplets in Electrospray Ionization and Their Influence on Chemical Equilibria. *J. Am. Soc. Mass Spectrom.* **2007**, *18* (3), 385−393.
(27) Quiros, I.; Yamada, M.; Kubo, K.; Mizutani, J.; Kurihara, M.; Nishihara, H. Preparation of alkanethiolate-protected palladium nanoparticles and their size dependence on synthetic conditions. *Langmuir* **2002**, *18* (4), 1413−1418.
(28) Björneholm, O.; Hansen, M. H.; Hodgson, A.; Liu, L.-M.; Limmer, D. T.; Michaelides, A.; Pedevilla, P.; Rossmeisl, J.; Shen, H.; Tocci, G.; Tyrode, E.; Walz, M.-M.; Werner, J.; Bluhm, H. Water at Interfaces. *Chem. Rev.* **2016**, *116* (13), 7698−7726.
(29) Shoji, T.; Shibata, M.; Kitamura, N.; Nagasawa, F.; Takase, M.; Murakoshi, K.; Nobuhiro, A.; Mizumoto, Y.; Ishihara, H.; Tsuboi, Y. Reversible photoinduced formation and manipulation of a two-dimensional closely packed assembly of polystyrene nanospheres on a metallic nanostructure. *J. Phys. Chem. C* **2013**, *117* (6), 2500−2506.
(30) Melcher, J. R.; Taylor, G. I. Electrohydrodynamics: A Review of the Role of Interfacial Shear Stresses. *Annu. Rev. Fluid Mech.* **1969**, *1* (1), 111−146.

DOI: 10.1021/acs.jpcc.8b04169
J. Phys. Chem. C 2018, 122, 17777−17783